3-23-2015

Applied Quantum Chemistry: Spectroscopic Detection and Characterization of the F_2BS and Cl_2BS Free Radicals in the Gas Phase

Bing Jin
University of Kentucky, bing.jin@uky.edu

Phillip M. Sheridan
Canisius College

Dennis J. Clouthier
University of Kentucky, dclaser@uky.edu

Applied Quantum Chemistry: Spectroscopic Detection and Characterization of the F_2BS and Cl_2BS Free Radicals in the Gas Phase

Digital Object Identifier (DOI)
http://dx.doi.org/10.1063/1.4915126

Applied quantum chemistry: Spectroscopic detection and characterization of the F_2BS and Cl_2BS free radicals in the gas phase

Bing Jin,[1] Phillip M. Sheridan,[2] and Dennis J. Clouthier[1,a)]
[1]*Department of Chemistry, University of Kentucky, Lexington, Kentucky 40506-0055, USA*
[2]*Department of Chemistry and Biochemistry, Canisius College, Buffalo, New York 14208, USA*

(Received 29 January 2015; accepted 5 March 2015; published online 23 March 2015)

In this and previous work [D. J. Clouthier, J. Chem. Phys. **141**, 244309 (2014)], the spectroscopic signatures of the X_2BY (X = H, halogen, Y = O, S) free radicals have been predicted using high level *ab initio* theory. The theoretical results have been used to calculate the electronic absorption and single vibronic level (SVL) emission spectra of the radicals under typical jet-cooled conditions. Using these diagnostic predictions, the previously unknown F_2BS and Cl_2BS free radicals have been identified and characterized. The radicals were prepared in a free jet expansion by subjecting precursor mixtures of BF_3 or BCl_3 and CS_2 vapor to an electric discharge at the exit of a pulsed molecular beam valve. The $\tilde{B}^2A_1$–$\tilde{X}\ ^2B_2$ laser-induced fluorescence spectra were found within 150 cm^{-1} of their theoretically predicted positions with vibronic structure consistent with our Franck-Condon simulations. The $\tilde{B}^2A_1$ state emits down to the ground state and to the low-lying $\tilde{A}^2B_1$ excited state and the correspondence between the observed and theoretically derived SVL emission Franck-Condon profiles was used to positively identify the radicals and make assignments. Excited state Coriolis coupling effects complicate the emission spectra of both radicals. In addition, a forbidden component of the electronically allowed $\tilde{B}$–$\tilde{X}$ band system of Cl_2BS is evident, as signaled by the activity in the b_2 modes in the spectrum. Symmetry arguments indicate that this component gains intensity due to a vibronic interaction of the $\tilde{B}^2A_1$ state with a nearby electronic state of $^2B_2$ symmetry. © *2015 AIP Publishing LLC*. [http://dx.doi.org/10.1063/1.4915126]

I. INTRODUCTION

Free radicals of the general formula X_2BY (X = H, D or halogen, Y = O, S) are little known, although boron-containing free radicals are important intermediates in a variety of contexts. For example, boron has been characterized as a key element in radical reactions where organoboron species are used as radical initiators, chain-transfer reagents, and radical precursors.[1] In addition, boron halides and simple boranes are used as boron sources in chemical vapor deposition processes for the production of boron nitrides, carbides, and amorphous boron thin films and boron-centered free radicals are likely intermediates in such processes. The high temperature chemistry of boron rocket fuel additives also involves free radical reactions.[2] Discoveries of new boron-containing free radicals are both relevant and significant in all these areas of chemistry. In the present work, aided by *ab initio* predictions of their spectroscopic properties, we report the first detection of two new species, the planar F_2BS and Cl_2BS free radicals.

The only X_2BY radicals previously known were the F_2BO and H_2BO species. In 1965, Mathews and Innes[3] presented spectroscopic evidence that F_2BO was the mostly likely source of an emission band system at 580 nm that was obtained from discharges through BF_3/O_2 mixtures. In 1966, Mathews[4] showed that a group of closely spaced red-degraded emission bands at 446.5 nm obtained in the same discharge was also due to F_2BO (or possibly F_2BO^+). The author could not definitively establish if the 580 nm and 446.5 nm bands had a common electronic state or if either band system involved transitions to the ground state. Subsequently, Dixon *et al.*[5] compared these bands with those of F_2CN and eliminated F_2BO^+ as a possible source of the 580 and 446.5 nm band systems. Finally, in 1988, Jacox[6] reconsidered Mathews' data and postulated that the 446.5 nm system was due to the $1^2A_1 \rightarrow \tilde{X}^2B_2$ transition and that the 580 nm bands were transitions from the same upper state to a low-lying excited state ($1^2A_1 \rightarrow 1^2B_1$), assignments which were subsequently supported by detailed *ab initio* calculations.[7]

In 2014, we reported the first laser-induced fluorescence (LIF) and emission spectra of jet-cooled $F_2{}^{11}BO$ and $F_2{}^{10}BO$ obtained by laser excitation of the bands near 446.5 nm.[8] F_2BO was generated in a pulsed discharge jet apparatus, using a precursor mixture of 7% BF_3 and 7% O_2 in high pressure argon. The emission spectrum obtained by laser excitation of the 0-0 band clearly showed transitions down to the ground state and a second set of bands down to the low-lying excited state, precisely as postulated by Jacox.[6] Our combined experimental and *ab initio* results proved conclusively that the previously reported emission spectra[4,5] were due to F_2BO and substantially extended our knowledge of the structure, vibrational frequencies, and electronic states of this interesting free radical.

The only other study of an X_2BY radical was the 1976 report by Graham and Weltner[9] of the detection of the

a)Author to whom correspondence should be addressed. Electronic mail: dclaser@uky.edu

H_2BO radical among the products produced by vaporizing and trapping elemental boron in solid argon at 4-10 K. It was identified by its ESR spectrum, which was very similar to that of the isoelectronic H_2CN free radical.[10] No further experimental observations of H_2BO species have been reported and the Cl_2BO, Br_2BO, H_2BS, F_2BS, Cl_2BS, and Br_2BS free radicals have never been previously observed.

In anticipation of the possibility of finding new X_2BY radicals, Clouthier[11] conducted an extensive *ab initio* study of the ground and first two excited electronic states of the H_2BO, H_2BS, F_2BO, and F_2BS free radicals and their various isotopologues. The radicals were found to have planar C_{2v} geometries in the $\tilde{X}^2B_2$ ground state, the low-lying $\tilde{A}^2B_1$ first excited state, and the higher $\tilde{B}^2A_1$ state. The most promising method of identifying these species in the gas phase was suggested to be absorption or laser-induced fluorescence spectroscopy through the allowed $\tilde{B} - \tilde{X}$ transitions which occur in the visible-near UV region of the electromagnetic spectrum. Complete basis set extrapolations of CCSD(T)/aug-cc-pVXZ (X = 3,4,5) energies were used to accurately predict the excited state energies. Franck-Condon profiles of the absorption and emission spectra and the rotational structure of the $\tilde{B} - \tilde{X}\ 0_0^0$ bands were simulated from the *ab initio* results. The calculated single vibronic level (SVL) emission spectra were found to provide a unique, readily recognizable fingerprint of each particular radical, facilitating the experimental identification of new X_2BY species in the gas phase. These predictions were very successfully employed in the present work to identify F_2BS and similar calculations led us to the Cl_2BS radical.

II. EXPERIMENT

F_2BS and Cl_2BS were generated in our pulsed discharge jet apparatus, which has been described elsewhere,[12] using precursor mixtures of 4% BF_3 or BCl_3 and 4% CS_2 in high pressure argon. In brief, the precursor gas was injected with a pulsed valve into an evacuated flow channel in a vacuum chamber. At the appropriate time, the gas pulse was subjected to a pulsed electric discharge between a pair of stainless steel ring electrodes placed in the flow channel, fragmenting the precursor molecules and producing products. A short 1 cm long reheat tube[13] was added to the flow channel downstream of the electrodes to increase the number of collisions and enhance the production of the radicals. Natural abundance BF_3 or BCl_3 (80% ^{11}B and 20% ^{10}B, Matheson) were used to measure transitions for the boron-11 isotopologue, while isotopically enriched $^{10}BF_3$ (96%, Ceradyne Boron Products) was used for measurements on $F_2{}^{10}BS$. $^{10}BCl_3$ was synthesized by the reaction of gaseous $^{10}BF_3$ with powdered $AlCl_3$ at elevated temperatures, in a modified literature procedure,[14] and used for studies of $Cl_2{}^{10}BS$.

Approximately, 1 cm downstream of the reheat tube, the free jet expansion was interrogated with the beam of a tunable dye laser (Nd:YAG pumped Lumonics HD-500) to obtain modest resolution (~0.1 cm^{-1}) LIF spectra. The fluorescence was imaged onto the photocathode of a high-gain photomultiplier (EMI 9816QB), and the pulsed signals were processed with a gated integrator, digitized by a National Instruments A/D board, and recorded with LabVIEW based software. The LIF spectra were calibrated to ±0.1 cm^{-1} using a portion of the laser beam to simultaneously record the neon and argon optogalvanic spectra using hollow cathode lamps.

For low-resolution SVL emission spectra, fluorescence was generated by pumping the maximum of an LIF band and then the emission was focused through $f/1.5$ optics onto the entrance slit of a scanning monochromator (Spex 500M). The spectra were calibrated to an estimated ±1 cm^{-1} accuracy using emission lines from an argon-filled hollow cathode lamp. The monochromator was equipped with an 1800 lines/mm grating blazed at 400 nm and operated with a bandpass of 0.2-0.8 nm.

The BS_2 radical was also produced in our discharge and its strong fluorescence interfered with our studies of the LIF spectra. As in previous work,[8] we used both time-gating and synchronously scanning (sync-scan) LIF techniques to isolate the signals of the radicals of interest. The sync-scan LIF method used a monochromator as a tunable bandpass filter by synchronously scanning the monochromator and the excitation laser with a fixed wavenumber offset between the two. In this fashion, we were able to isolate fluorescence from the species of interest, largely free of impurity emission.

III. RESULTS AND ANALYSIS

A. *Ab initio* calculations on Cl_2BS

Our success in identifying F_2BS based on a*b initio* predictions of the LIF and emission spectra[11] (*vide infra*) encouraged us to undertake similar theoretical studies of Cl_2BS. Due to the larger number of electrons, these were not as extensive as the complete basis set extrapolations previously performed for the smaller H_2BO, H_2BS, F_2BO, and F_2BS radicals,[11] but were of sufficient quality to lead to unambiguous predictions of the expected spectra. In the present work, the ground and two lowest energy excited electronic states were examined with density functional theory (DFT) using the Becke 3-parameter exchange and Lee-Yang-Parr correlation (B3LYP) hybrid functional[15,16] and coupled cluster theory with singles, doubles, and perturbatively included triples [CCSD(T)] using Dunning's correlation consistent basis sets augmented with diffuse functions[17] (aug-cc-pVnZ). The basis sets for chlorine and sulfur included a further tight *d* function [aug-cc-pV(X+d)Z] which facilitated convergence.[18] All the *ab initio* calculations were done with the Gaussian 09 software package.[19] The three electronic states were calculated variationally by constraining the geometry to C_{2v} symmetry, with each state exhibiting a minimum on the potential energy surface. The highest level CCSD(T)/aug-cc-pV(T+d)Z vibrational frequencies and T_0 values are presented in Table I, with the geometric parameters relegated to Table VII. As in previous work,[11] the vibrational frequencies are numbered conventionally such that the vibrations are segregated by symmetry species and numbered in order of decreasing frequency within each symmetry species, so that ν_1, ν_2, and ν_3 are the a_1 modes, ν_4 is the single b_1 mode, and ν_5 and ν_6 are the b_2 modes.

The *ab initio* calculations show that the ground state electronic configuration of Cl_2BS is $\ldots(13a_1)^2\ (4b_1)^2\ (9b_2)^1$, which gives rise to a $^2B_2$ term. The $9b_2$ HOMO is essentially

TABLE I. Summary of the observed vibrational fundamentals and T_0 values and the corresponding *ab initio* (in parentheses) harmonic frequencies for the various electronic states of F_2BS and Cl_2BS (in cm^{-1}).

		T_0	$\nu_1(a_1)$	$\nu_2(a_1)$	$\nu_3(a_1)$	$\nu_4(b_1)$	$\nu_5(b_2)$	$\nu_6(b_2)$
$\tilde{X}^2B_2$	$F_2{}^{11}BS$	...	1232 (1242)[a]	683 (683)	412 (410)	578 (578)	... (1398)	276 (277)
	$F_2{}^{10}BS$	...	1275 (1285)	684 (687)	413 (410)	598 (602)	1452 (1447)	279 (279)
	$Cl_2{}^{11}BS$	...	960 (966)[b]	462 (464)	237 (239)	... (432)	910 (922)	179 (181)
	$Cl_2{}^{10}BS$	...	1000 (1006)	464 (464)	240 (239)	... (451)	946 (959)	180 (182)
$\tilde{A}^2B_1$	$F_2{}^{11}BS$	3 517 (3 464)	1224 (1236)	657 (660)	415 (420)	545 (545)	... (1412)	... (316)
	$F_2{}^{10}BS$	3 520 (3 463)	1248 (1277)	659 (666)	415 (420)	562 (568)	... (1462)	... (318)
	$Cl_2{}^{11}BS$	4 862 (4 769)	901 (909)	443 (453)	256 (255)	... (409)	932 (942)	231 (232)
	$Cl_2{}^{10}BS$	4 865 (4 768)	940 (947)	448 (453)	253 (256)	... (427)	968 (981)	231 (233)
$\tilde{B}^2A_1$	$F_2{}^{11}BS$	23 180 (23 175)	1101 (1136)	610 (617)	395 (394)	573 (579)	... (1509)	318 (319)
	$F_2{}^{10}BS$	23 180 (23 174)	1135 (1167)	621 (625)	399 (394)	599 (603)	... (1564)	324 (320)
	$Cl_2{}^{11}BS$	21 123 (21 271)	746 (756)	454 (453)	243 (240)	... (433)	960 (986)	256 (256)
	$Cl_2{}^{10}BS$	21 123 (21 269)	774 (787)	456 (454)	246 (242)	... (452)	998 (1027)	257 (256)

[a]F_2BS CCSD(T)/aug-cc-pV5Z results from Ref. 11.
[b]Cl_2BS CCSD(T)/aug-cc-pVTZ results, present work.

an in-plane *p* orbital on the sulfur atom and can be labeled as nonbonding (n_O). The $4b_1$ second highest occupied molecular orbital (SHOMO) is the out-of-plane *p* orbital on the sulfur atom with some stabilization from the out-of-plane *p* orbital on the boron atom, and so can be termed a π_{BS} orbital. Finally, the $13a_1$ third highest occupied molecular orbital (THOMO) is a slightly bonding orbital between the boron and sulfur atoms, which can be labeled σ_{BO}. Parenthetically, we note that the ground state dipole moment of Cl_2BS is predicted to be about 0.4 D, which may make microwave observations difficult. The ν_1 and ν_5 fundamentals have appreciable infrared absorption intensities (175–270 km/mol), so it might be possible to detect Cl_2BS in matrix isolation experiments in the 800–1000 cm^{-1} region.

Promoting a single electron from the SHOMO to the HOMO produces the low-lying $\tilde{A}^2B_1$ state, which has a somewhat longer B–S bond length (increase of ~0.06 Å) due to the removal of an electron from an orbital with π bonding character between these two atoms. The $\tilde{B}^2A_1$ state is formed from the promotion of an electron in the THOMO to the HOMO, which can be considered an n–σ transition, which again increases the B–S bond length by 0.03–0.06 Å depending on the level of theory.

We have also used our CCSD(T)/aug-cc-pVTZ *ab initio* results to perform Franck-Condon simulations of the absorption and single vibronic level emission spectra of Cl_2BS, as an aid to the experimental identification. The simulation program, originally developed by Yang *et al.*,[20] and locally modified for the calculation of SVL emission spectra, requires input of the molecular structures, vibrational frequencies, and mass-weighted Cartesian displacement coordinates from the *ab initio* force fields of the two combining electronic states. Franck-Condon factors are then calculated in the harmonic approximation using the exact recursion relationships of Doktorov *et al.*[21] taking into account both normal coordinate displacement and Duschinsky rotation effects.

B. Spectra of F_2BS

The LIF spectrum of $F_2{}^{11}BS$ is shown in Fig. 1. It commences with a strong 0-0 band centered at 23 178.5 cm^{-1}, fortuitously close to T_0 = 23 175 cm^{-1} predicted in our previous *ab initio* study.[11] The inset in Fig. 1 shows that the calculated 0-0 band contour, obtained from the *ab initio* rotational constants, matches experiment very well and validates our prediction that the band should follow *b*-type

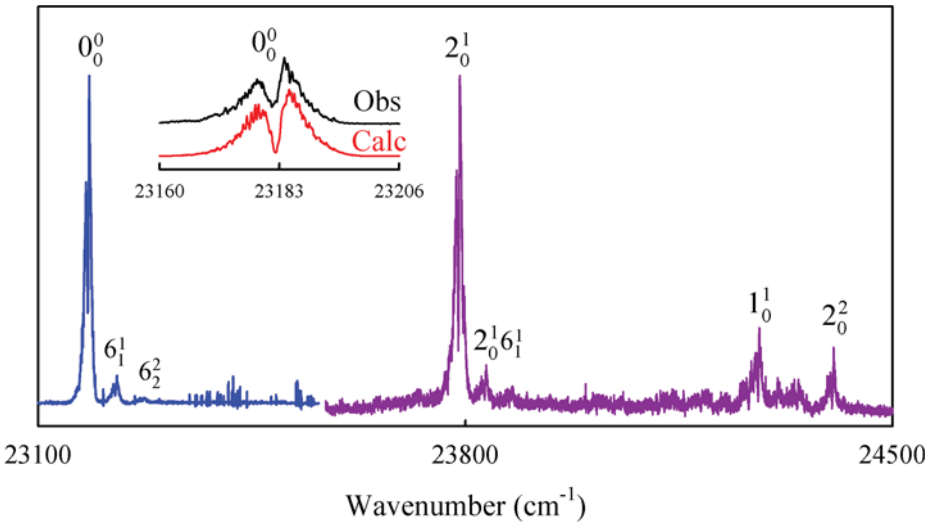

FIG. 1. The low resolution LIF spectrum of the $\tilde{B}$–$\tilde{X}$ transition of F_2BS. The spectrum was recorded in two sections with different laser dyes so the relative intensities of the two segments are not meaningful. The inset shows the observed and calculated (from our B3LYP/aug-cc-pV5Z results) rotational contours of the $F_2{}^{11}BS$ 0-0 band.

selection rules.[11] Our Franck-Condon simulation[11] of the LIF cold band spectrum shows a very strong 0-0 band, and weaker 2_0^1 and 1_0^1 bands along with a few very weak transitions and this is essentially what is observed. In addition, the experimental spectrum exhibits a few weak hot bands (2_1^1, 3_1^1, 6_1^1, 6_2^2, $2_0^1 3_1^1$, and $2_0^1 6_1^1$, not all identified in Fig. 1), analogous to those found in the spectrum of F_2BO.[8] The LIF spectrum of $F_2{}^{10}BS$ is very similar to that shown in Fig. 1, although the 1_0^1 band is shifted 30 cm^{-1} to higher energy, in complete agreement with the *ab initio* isotope shift of 30 cm^{-1}. There can be little doubt that the observed LIF spectrum is the $\tilde{B}^2A_1$–$\tilde{X}^2B_2$ band system of F_2BS. A list of the observed LIF bands is given in Table II.

Unequivocal proof that F_2BS is the carrier of the LIF spectrum in Fig. 1 comes from the comparison of the observed and calculated 0-0 band emission spectra, shown in Fig. 2. In fact, the correspondence between the experimental spectrum and the Franck-Condon simulation is so good that the majority of the bands were assigned directly from their simulation counterparts. The $\tilde{B}$–$\tilde{X}$ emission spectrum of $F_2{}^{11}BS$ consists of a relatively small number of bands (11) with a prominent progression in ν_1'' out to 1_2^0, consistent with the 0.06 Å difference in the BS bond length in the two states. The arrows in Fig. 2 highlight three features not reproduced in the simulation. Bands #2 and #3 are the 1_1^0 and 1_2^0 transitions of $F_2{}^{10}BS$ present in 20% natural abundance, which are resolved from the $F_2{}^{11}BS$ bands due to the relatively large ν_1'' (B–S stretching) isotope effect (see Table I). Both show up prominently in the spectrum of isotopically enriched $F_2{}^{10}BS$. Band #1 cannot be attributed to $F_2{}^{10}BS$, although a similar very weak band occurs 50 cm^{-1} higher in energy in the spectrum of $F_2{}^{10}BS$. The only other ground state vibration with frequency lower than ν_1 and with a significant boron isotope effect is ν_4 with a calculated ^{11}B frequency of 578 cm^{-1} and isotope shift of 24 cm^{-1} (see Table I). We therefore tentatively assign this transition to the 4_2^0 band, with half the interval giving

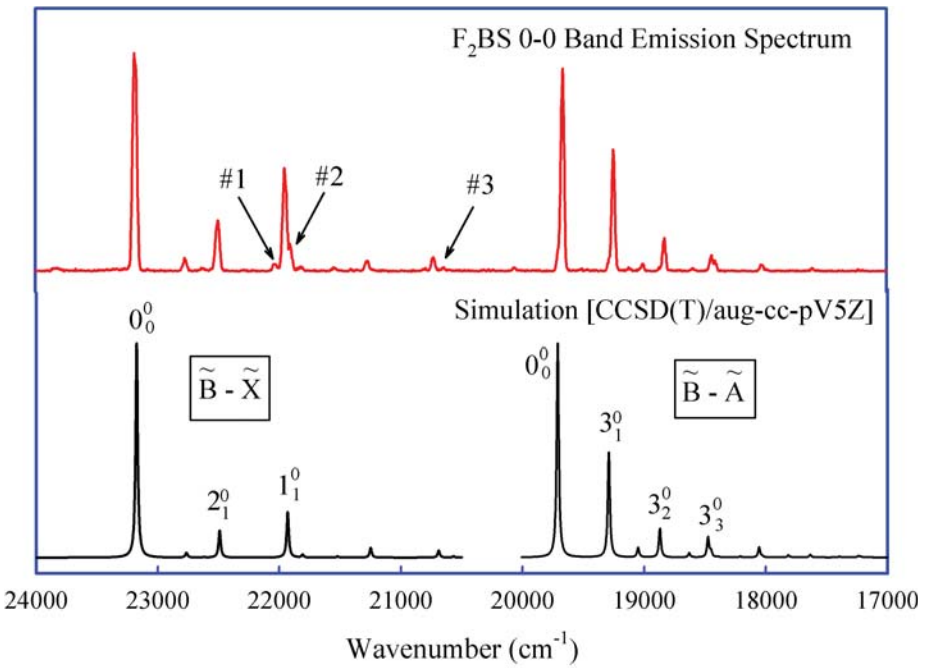

FIG. 2. The observed 0-0 band emission spectrum of F_2BS (top panel) and the corresponding harmonic Franck-Condon simulation (bottom panel). The simulations involved calculating the $\tilde{B}$-$\tilde{X}$ and $\tilde{B}$-$\tilde{A}$ spectra, separately, so there is a break in the spectrum near 20 300 cm^{-1}. The relative intensities of the two calculated spectra have been normalized to the strongest feature in the corresponding emission spectrum.

TABLE II. Observed vibronic bands in the LIF spectra of the $\tilde{B}\ ^2A_1$–$\tilde{X}\ ^2B_2$ transition of the boron isotopologues of F_2BS.

	$F_2{}^{11}BS$		$F_2{}^{10}BS$	
Assignment	Transition (cm^{-1})	Interval (cm^{-1})	Transition (cm^{-1})	Interval (cm^{-1})
2_1^1	...	...	23 116.3	$0_0^0-58.5$
3_1^1	23 161.3	$0_0^0-17.2$	23 160.8	$0_0^0-14.0$
0_0^0	23 178.5	...	23 174.8	...
6_1^1	23 220.9	$0_0^0+42.4$	23 220.1	$0_0^0+45.3$
6_2^2	23 266.1	$6_1^1+45.2$	...	...
$2_0^1 3_1^1$	23 771.0	$3_1^1+609.7$	23 777.7	$3_1^1+616.9$
$2_0^1/4_0^1$	23 788.6	$0_0^0+610.1$	23 795.8	$0_0^0+621.0$
$2_0^1 6_1^1$	23 831.7	$6_1^1+610.8$	23 838.1	$6_1^1+618.0$
1_0^1	24 279.7	$0_0^0+1101.2$	24 309.9	$0_0^0+1135.1$
2_0^2	24 400.9	$2_0^1+612.3$	24 417.0	$2_0^1+621.2$

TABLE III. Emission bands (in cm^{-1}) observed by pumping the 0_0^0 and 2_0^1 absorption bands of the $\tilde{B}$–$\tilde{X}$ transition of F_2BS. Unassigned lines: $F_2{}^{10}BS$: 0-0 band spectrum 20 063(vw); 2(1,0) band spectrum 20 028 (w).

	0_0^0 band emission spectrum				2_0^1 band emission spectrum				
	$F_2{}^{11}BS$		$F_2{}^{10}BS$		$F_2{}^{11}BS$			$F_2{}^{10}BS$	
Assign	Transition	Interval	Transition	Interval	Assign	Transition	Interval	Transition	Interval
				$\tilde{B}-\tilde{X}$ transitions[a]					
0_0^0	23 181	...	23 180	...	2_0^1	23 796	$\nu'_2=615$	23 802	$\nu'_2=622$
3_1^0	22 769	$\nu_3=412$	22 767	$\nu_3=413$	4_1^1	23 181	...	23 183	...
6_2^0	22 629	$2\nu_6=552$	22 621	$2\nu_6=559$	2_1^1	23 113	$\nu_2=683$	23 117	$\nu_2=685$
2_1^0	22 500	$\nu_2=681$	22 496	$\nu_2=684$	$2_1^1 3_1^0$	22 711	$\nu_3=402$	22 710	$\nu_3=407$
4_2^0?	22 031	$2\nu_4=1150$	21 981	$2\nu_4=1199$	$2_1^0 4_1^1$	22 506	$\nu_2=675$	22 501	$\nu_2=682$
1_1^0	21 949	$\nu_1=1232$	21 904	$\nu_1=1276$	2_2^1	22 438	2_1^1-675	22 436	2_1^1-681
2_2^0	21 811	2_1^0-689	...	...	$1_1^0 4_1^1$	21 956	4_1^1-1225	21 904	4_1^1-1279
$1_1^0 3_1^0$	21 546	1_1^0-403	21 504	1_1^0-400	$1_1^0 2_1^1$	21 884	2_1^1-1229	21 846	2_1^1-1271
$1_1^0 2_1^0$	21 273	1_1^0-676	21 227	1_1^0-677	2_3^1	21 752	2_2^1-686	...	...
$1_1^0 4_2^0$?	...	...	20 711	1_1^0-1193	$1_1^0 2_2^1$	21 214	2_2^1-1224	21 168	2_2^1-1268
1_2^0	20 728	1_1^0-1221	20 642	1_1^0-1262	$1_2^0 4_1^1$	...	...	20 641	4_1^1-2542
5_2^0?	...	...	20 275	$2\upsilon_5=2905$	$1_2^0 2_1^1$	20 657	2_1^1-2456	20 584	2_1^1-2533
$1_2^0 2_1^0$	20 061	1_2^0-667	...	2 ...	$1_2^0 2_1^0 4_1^1$	20 028	...	...	...
				$\tilde{B}-\tilde{A}$ transitions[b]					
0_0^0	19 664	$\tilde{X}0_0+3517$	19 660	$\tilde{X}0_0+3520$	2_0^1	20 278	$\nu'_2=614$	20 283	$\nu'_2=623$
3_1^0	19 249	$\nu_3=415$	19 245	$\nu_3=415$	$2_0^1 3_1^0$	19 862	$\nu_3=416$	19 865	$\nu_3=418$
2_1^0	19 004	$\nu_2=660$	19 006	$\nu_2=654$	4_1^1	19 695	...	19 699	...
3_2^0	18 829	3_1^0-420	18 828	3_1^0-417	2_1^1	19 620	$\nu_2=658$	19 624	$\nu_2=659$
$2_1^0 3_1^0$	18 592	2_1^0-412	...	...	$3_1^0 4_1^1$	...	...	19 281	4_1^1-418
1_1^0	18 440	$\nu_1=1224$	18 412	$\nu_1=1248$	$2_1^1 3_1^0$	19 206	2_1^1-414	19 207	2_1^1-417
3_3^0	18 410	3_2^0-419	...	...	$2_1^0 4_1^1$	...	...	19 037	4_1^1-662
...	...	...	...	...	2_2^1	18 962	2_1^1-658	18 966	2_1^1-658
...	...	...	...	...	$3_2^0 4_1^1$	...	...	18 863	4_1^1-836
$1_1^0 3_1^0$	18 028	1_1^0-412	17 990	1_1^0-422	$2_1^1 3_2^0$	18 792	2_1^1-828	18 791	2_1^1-833
...	...	...	...	...	$1_1^0 4_1^1$	...	...	18 442	4_1^1-1257
...	...	...	...	...	$1_1^0 2_1^1$	18 398	2_1^1-1222	18 371	2_1^1-1253
$1_1^0 3_2^0$	17 612	$1_1^0 3_1^0-416$	...	...	$1_1^0 2_1^1 3_1^0$	17 987	...	...	...

[a]Vibrational intervals are for the $\tilde{X}$ state unless otherwise noted.
[b]Vibrational intervals are for the $\tilde{A}$ state unless otherwise noted.

$\nu_4'' = 575\ cm^{-1}$ and a 25 cm^{-1} isotope shift. The 0-0 band emission spectrum of $F_2{}^{10}BS$ has many of the same features but has additional very weak bands tentatively assigned as $1_1^0 4_2^0$ and 5_2^0. Since transitions involving two quanta of non-totally symmetric modes are expected to be very weak, all such assignments are only tentative as they could also be due to impurities or emission from higher levels excited through sequence bands overlapping the 0-0 band. A complete list of the $\tilde{B}$–$\tilde{X}$ emission band assignments is given in Table III.

The 0-0 band $\tilde{B}$–$\tilde{A}$ emission band systems of $F_2{}^{11}BS$ and $F_2{}^{10}BS$ were very easy to assign as they matched the simulations almost perfectly, with no extraneous features. The major progression involves ν_3 (out to 3_3^0) with a small amount of activity in ν_1. Animations show that in the $\tilde{A}$ state both of these modes involve substantial contributions from the BS stretching and FBF symmetric bending internal coordinates. The assignments are summarized in Table III.

We also recorded the SVL emission spectra of the 2_0^1 bands, which harbored a surprise. In this case, the emission spectra were much more complicated than the initial simulation, with some bands consisting of closely spaced doublets (particularly for $F_2{}^{10}BS$) along with a few extraneous features. Examining the $\tilde{B}$ state calculated vibrational frequencies (Table I), it is apparent that ν_2 and ν_4 are almost degenerate, differing by 38 cm^{-1} in $F_2{}^{11}BS$ and only 22 cm^{-1} in $F_2{}^{10}BS$ and that Coriolis coupling between the $\tilde{B}$ state 2^1 and 4^1 levels is the likely reason for the complexity. The 2_0^1 band emission spectrum of $F_2{}^{10}BS$ is shown in Fig. 3, along with a simulation constructed by adding together Franck-Condon simulations from the 2^1 and 4^1 levels and normalizing the intensities to those of the observed 4_1^1 and 2_1^1 bands in each case. The agreement is excellent, confirming that the upper state pumped by the laser has $2^1/4^1$ character. The bands in the spectra of both isotopologues were assigned based on observed and calculated vibrational intervals and on the relative intensities predicted by the composite simulations. These results are summarized in Table III.

C. Spectra of Cl_2BS

Our best CCSD(T)/aug-cc-pVTZ calculations predicted the $\tilde{B}$–$\tilde{X}$ T_0 of $Cl_2{}^{11}BS$ to be 21 271 cm^{-1}. Substituting BCl_3 for BF_3 and using similar experimental conditions, we readily found a strong 0-0 band at 21 123 cm^{-1}, 148 cm^{-1} lower than predicted. The Franck-Condon simulation of the Cl_2BS cold band absorption spectrum indicates that there should be more bands than observed in the LIF spectra of F_2BO and F_2BS, which is what is found, as shown in Fig 4. In addition to the very strong 0-0 band, there are weaker 3_0^1, 2_0^1, 1_0^1, and combination bands. Furthermore, the spectra of both isotopologues exhibit weak hot bands below 21 000 cm^{-1} which can only be assigned as 3_1^0 and 6_1^0. The latter is unprecedented in the LIF spectra of the fluorinated radicals and must be vibronically induced through mixing with another excited state. The corresponding 6_0^1 cold band is calculated to lie within the rotational envelope of the noticeably broad 3_0^1 band (FWHM: $0_0^0 \approx 9\ cm^{-1}$, $3_0^1 \approx 19\ cm^{-1}$). In addition, $Cl_2{}^{11}BS/Cl_2{}^{10}BS$ shows a weak band 960/998 cm^{-1} above the 0_0^0 band which is assigned as the vibronically induced 5_0^1 band, based on detailed consideration of the emission data (*vide infra*). Of course, ν_5' has the same vibrational symmetry as ν_6'', so it is perhaps not too surprising that 5_0^1 also appears in the Cl_2BS spectrum. Finally, the Cl_2BS least moment of inertia (I_a) is in the molecular plane perpendicular to the B–S bond, so the bands should follow *a*-type selection rules and not exhibit the central minima found for F_2BS (see Fig. 1), and this is what is observed. The assignments of the LIF spectra are given in Table IV along with some derived vibrational intervals.

The substantial number of bands in the LIF spectra provided the opportunity to obtain many more SVL emission

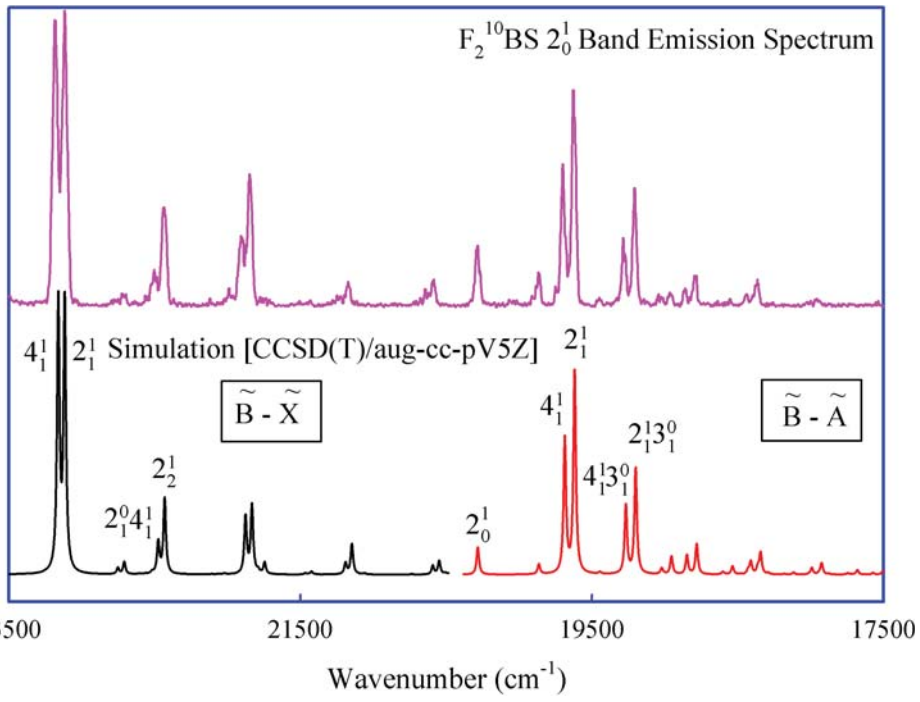

FIG. 3. The $F_2{}^{10}BS$ 2_0^1 band emission spectrum (top panel) and the corresponding harmonic Franck-Condon simulation (bottom panel). The simulation was obtained by adding together Franck-Condon simulations of emission spectra from the 2^1 and 4^1 levels and normalizing the intensities to those of the observed 4_1^1 and 2_1^1 bands in each case.

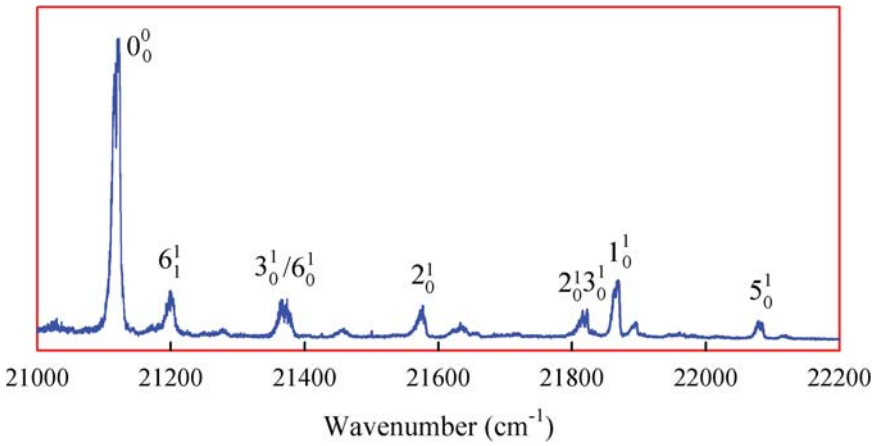

FIG. 4. A portion of the low resolution LIF spectrum of the $\tilde{B}$-$\tilde{X}$ transition of Cl_2BS. The 3(1,0) and 6(1,0) bands are overlapped, giving rise to a feature that appears to be broader than any other in the spectrum.

spectra than in the F_2BO and F_2BS cases. For each isotopologue, we recorded dispersed emission spectra by pumping the 3_1^0, 6_1^0, 0_0^0, 6_1^1, $3_0^1/6_0^1$, $6_1^1 3_0^1$, 2_0^1, 1_0^1, and 5_0^1 LIF bands, along with the $2_0^1 3_0^1$ band of $Cl_2{}^{11}BS$ and the 6_0^2 band of $Cl_2{}^{10}BS$. We will not discuss the details of all these spectra but simply refer to a few cases which illustrate the salient points of the analysis.

The 0-0 band emission spectrum of $Cl_2{}^{11}BS$ is shown in Fig. 5 along with our Franck-Condon simulation. It is readily apparent that the simulation is substantially at odds with experiment for the $\tilde{B}$–$\tilde{X}$ band system but is in quite good agreement for the $\tilde{B}$–$\tilde{A}$ transitions. The small features labeled #1, #2 and #3 are the key to understanding this behavior. Transitions #1 and #2 are to higher energy than the 0-0 band that was pumped by the laser and are readily assigned as 3_0^1 and 6_1^1, both bands that are also observed in the LIF spectra. We conclude that the 0-0 band is overlapped by the 3_1^1 sequence band (it is calculated from the known vibrational frequencies to occur within the rotational contour of the 0-0 band) and that the 3^1 (ν_3 = 244 cm^{-1}) and 6^1 (ν_6 = 259 cm^{-1}) levels are Coriolis coupled. A similar complication was found in the spectrum of F_2BO.[8] This conclusion is buttressed by the fact that pumping the Cl_2BS 6_1^1 band yields an emission spectrum that includes a weak 3_0^1 band. Thus, the 0-0 band emission spectrum in Fig. 5 contains contributions from the $\tilde{B}$ state 0^0, 3^1, and 6^1 levels, accounting for the deviations from the harmonic Franck-Condon simulation. In addition to the bands predicted by the Franck-Condon simulation, we have also assigned a weak vibronically induced 6_1^0 band and an even weaker $1_1^0 6_1^0$ band.

Initially, further $Cl_2{}^{11}BS/Cl_2{}^{10}BS$ zero-point $\tilde{B}$–$\tilde{X}$ emission bands of medium intensity with ground state intervals of 907/949 cm^{-1} were difficult to assign. However, once it was recognized that the strongest features of the emission spectra of the LIF bands at 22 078.3/22 114.3 cm^{-1} (Table IV) had the same intervals, it became apparent that these were the ν_5'' frequencies, with a boron isotope shift of 42 cm^{-1}, comparable to the *ab initio* value of 37 cm^{-1}. This assignment was confirmed by the presence of weak transitions down to the $1_1 5_1$ level in the 0_0^0 and 1_0^1 band emission spectra with observed $\nu_1 + \nu_5$ frequency isotope shifts of 79 cm^{-1} in both spectra. The expected isotope shift (from combining the observed shifts of

TABLE IV. Observed vibronic bands in the LIF spectra of the $\tilde{B}\ ^2A_1$–$\tilde{X}\ ^2B_2$ transition of the boron isotopologues of Cl_2BS.

	$Cl_2{}^{11}BS$		$Cl_2{}^{10}BS$	
Assignment	Transition (cm^{-1})	Interval (cm^{-1})	Transition (cm^{-1})	Interval (cm^{-1})
3_1^0	20 881.3	$\nu_3'' = 237.3$	20 878.8	$\nu_3'' = 237.5$
6_1^0	20 943.9	$\nu_6'' = 174.7$	20 940.0	$\nu_6'' = 176.3$
0_0^0	21 118.6	...	21 116.3	...
6_1^1	21 199.4	$\nu_6 = 255.5$	21 195.2	$\nu_6 = 255.2$
6_2^2	...	...	21 278.1	$6_1^1 + 82.9$
3_0^1 and 6_0^1	21 370.5	...	21 368.9	...
$3_0^1 6_1^1$	21 453.5	$6_1^1 + 254.1$	21 452.9	$6_1^1 + 257.7$
2_0^1	21 572.2	$\nu_2 = 453.6$	21 572.3	$\nu_2 = 456.0$
6_0^2 and 3_0^2?	21 633.9	...	21 632.6	...
$2_0^1 3_0^1$	21 817.2	$2_0^1 + 245.0$	21 814.1	$2_0^1 + 241.8$
1_0^1	21 863.9	$\nu_1 = 745.3$	21 889.8	$\nu_1 = 773.5$
5_0^1	22 078.3	$\nu_5 = 959.7$	22 114.3	$\nu_5 = 998.0$
$2_0^2 3_0^1$?	22 266.3	$2_0^1 3_0^1 + 449.1$	...	...
$1_0^1 2_0^1$	22 311.6	$2_0^1 + 739.4$	...	...

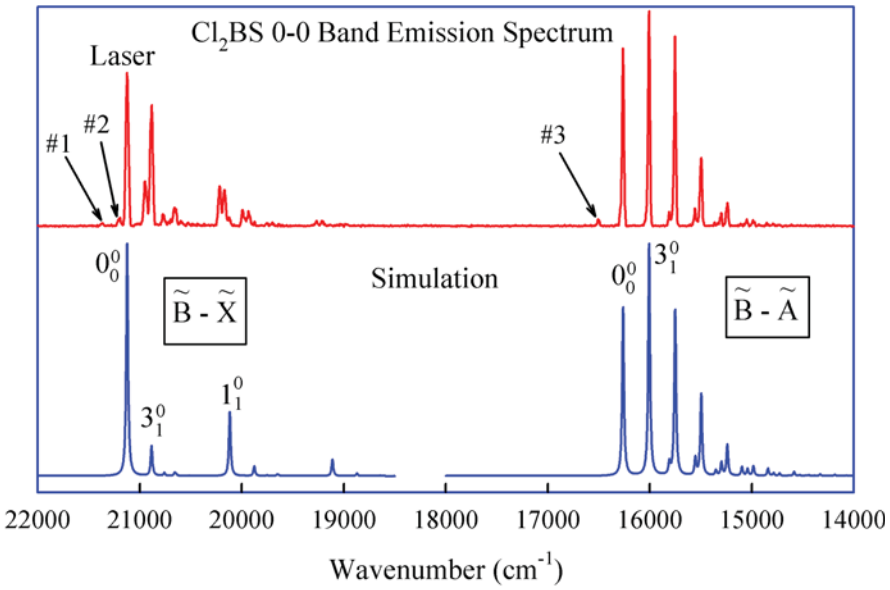

FIG. 5. The observed 0-0 band emission spectrum of Cl_2BS (top panel) and the corresponding harmonic Franck-Condon simulation (bottom panel). The simulations involved calculating the $\tilde{B}$-$\tilde{X}$ and $\tilde{B}$-$\tilde{A}$ spectra, separately, so there is a break in the spectrum near 18 500 cm^{-1}. The relative intensities of the two calculated spectra are not meaningful.

TABLE V. Emission bands observed by pumping the 0_0^0 band of the $\tilde{B}$–$\tilde{X}$ transition of Cl_2BS.

	$Cl_2{}^{11}BS$		$Cl_2{}^{10}BS$	
Assignment	Transition (cm^{-1})	Interval (cm^{-1})	Transition (cm^{-1})	Interval (cm^{-1})
		$\tilde{B}-\tilde{X}$[a]		
3_0^1	21 367	$\nu'_3 = 244$	21 374	$\nu'_3 = 251$
6_1^1	21 203	$\nu'_6 = 259$	21 200	$\nu'_6 = 259$
0_0^0	21 123	...	21 123	...
6_1^0	20 944	$\nu_6 = 179$	20 942	$\nu_6 = 181$
3_1^0	20 886	$\nu_3 = 237$	20 883	$\nu_3 = 240$
6_2^0	20 768	$6_1^0 - 176$	20 764	$6_1^0 - 178$
2_1^0	20 654	$\nu_2 = 469$	20 658	$\nu_2 = 465$
5_1^0	20 216	$\nu_5 = 907$	20 174	$\nu_5 = 949$
1_1^0	20 167	$\nu_1 = 956$	20 121	$\nu_1 = 1002$
$1_1^0 6_1^0$	19 992	$1_1^0 - 175$	19 945	$1_1^0 - 176$
$1_1^0 3_1^0$	19 927	$1_1^0 - 240$	19 884	$1_1^0 - 237$
$1_1^0 5_1^0$	19 263	$1_1^0 - 904$	19 184	$1_1^0 - 937$
1_2^0	19 209	$1_1^0 - 958$	19 135	$1_1^0 - 986$
$1_1^0 3_1^0 5_1^0$	...	...	18 954	$1_1^0 5_1^0 - 230$
		$\tilde{B}-\tilde{A}$[b]		
3_0^1	16 504	$\nu'_3 = 243$	16 504	$\nu'_3 = 246$
0_0^0	16 261	$\tilde{X}\ 0_0 + 4862$	16 258	$\tilde{X}\ 0_0 + 4865$
3_1^0	16 005	$\nu_3 = 256$	16 005	$\nu_3 = 253$
2(0,1)	15 809	$\nu_2 = 452$	15 813	$\nu_2 = 445$
3_2^0	15 753	$3_1^0 - 252$	15 750	$3_1^0 - 255$
$2_1^0 3_1^0$	15 557	$3_1^0 - 448$	15 555	$3_1^0 - 450$
3_3^0	15 495	$3_2^0 - 258$	15 494	$3_2^0 - 256$
$2_1^0 3_2^0$	15 301	$3_2^0 - 452$	15 303	$3_2^0 - 447$
3_4^0	15 239	$3_3^0 - 256$	15 238	$3_3^0 - 256$
$2_1^0 3_3^0$	15 045	$3_3^0 - 450$	15 051	$3_3^0 - 443$
3_5^0	14 986	$3_4^0 - 253$	14 986	$3_4^0 - 252$

[a]Vibrational intervals are for the $\tilde{X}$ state unless otherwise noted.
[b]Vibrational intervals are for the $\tilde{A}$ state unless otherwise noted.

ν_1'' and ν_5'') is 78 cm^{-1} whereas the *ab initio* value is 77 cm^{-1}, both in good agreement with experiment. The 0_0^0 band $\tilde{B}$–$\tilde{X}$ emission assignments are summarized in Table V.

Although the excellent agreement between Franck-Condon simulation and experiment (Fig. 5) shows that most of the intensity of the $\tilde{B}$–$\tilde{A}$ band system originates from the 0^0 level, the weak feature labeled #3 is not in the calculated spectrum, but was readily assigned as the 3_0^1 band. There is no evidence for any vibronically induced features in the $\tilde{B}$–$\tilde{A}$ spectrum. The most intense bands form a progression in ν_3'' out to 3_5^0, along with weaker bands involving ν_2'' and $\nu_2'' + \nu_3''$ combinations. These are listed in Table V.

Other emission spectra with upper states involving either ν_3' or ν_6' have similar complications due to the Coriolis coupling of these two modes. Most of the remaining emission spectra were understandable and assignable based on the assumption of laser excitation of a single uncompromised vibrational level, such as 1^1 or 2^1, with only modest deviations from the calculated spectra in the harmonic approximation, due to vibronically induced bands. Generally, it was found that the strongest features in the emission spectra of LIF bands involving an upper state fundamental (1_0^1, 2_0^1, etc.) were down to one quantum of the same fundamental in the ground state, in accord with expectations based on the Franck-Condon principle. Thus, the most intense $\tilde{B} - \tilde{X}$ emission bands from laser excitation of the 1^1, 2^1, 3^1, 5^1, and 6^1 levels were 1_1^1, 2_1^1, 3_1^1, 5_1^1, and 6_1^1, respectively.

From the analysis of the LIF and emission spectra, we have obtained most of the fundamental frequencies in the three combining states, as reported in Table I. Some of these values deserve further comment. The $\tilde{B}$ state ν_6 frequencies were obtained from the 6_1^1 to 6_1^0 LIF band intervals and the ground state ν_6 from the emission 0_0^0 to 6_1^0 differences. The $\tilde{A}$ state ν_6 values were calculated from the emission spectra as 0_0^0 ($\tilde{B} - \tilde{A}$) + ν_6' – 6_1^1 ($\tilde{B} - \tilde{A}$) and the ν_5 values were derived in a similar fashion. The $\tilde{B}$ state ν_3 values were taken as the differences between the $\tilde{B}$–$\tilde{A}$ 3_0^1 and 0_0^0 bands observed in the 0-0 band emission spectra, as the LIF values are compromised by the overlap of the 3_0^1 and 6_0^1 bands. In addition, a variety of Cl_2BS $\tilde{X}$ and $\tilde{A}$ state overtone and combination levels were measured and assigned and these are collected in Table VI.

TABLE VI. The observed overtone and combination vibrational intervals (in cm^{-1}) for the $\tilde{X}$ and $\tilde{A}$ electronic states of Cl_2BS.

	$\tilde{X}^2B_2$		$\tilde{A}^2B_1$	
	$Cl_2{}^{11}BS$	$Cl_2{}^{10}BS$	$Cl_2{}^{11}BS$	$Cl_2{}^{10}BS$
$2\nu_6$	355	355	...	...
$2\nu_3$	476	487	510	509
$\nu_3+2\nu_6$	...	596	...	...
$\nu_2+\nu_6$	631	633	...	...
$\nu_2+\nu_3$	700	702	704	703
$3\nu_3$	...	...	766	764
$2\nu_2$	930	933	893	904
$\nu_2+2\nu_3$	935	...	960	958
$4\nu_3$	...	...	1021	1020
$\nu_5+\nu_6$	1088	1121	...	...
$\nu_3+\nu_5$	1153	1181	1212	1249
$\nu_1+\nu_6$	1136	1178	...	...
$2\nu_2+\nu_3$	...	...	1150	1155
$\nu_1+\nu_3$	1197	1244	1155	1195
$\nu_2+3\nu_3$	...	...	1216	1216
$5\nu_3$	...	...	1275	1272
$\nu_2+\nu_5$	1368	1400	...	...
$\nu_1+\nu_2$	1417	1460	1351	1390
$2\nu_2+2\nu_3$	...	...	1398	...
$\nu_1+2\nu_3$	...	...	1412	1453
$\nu_2+4\nu_3$	...	...	1460	...
$2\nu_3+\nu_5$	...	...	1464	1517
$\nu_2+\nu_3+\nu_5$	1600	1636	1661	...
$\nu_1+\nu_2+\nu_3$	1654	1698	1605	1649
$\nu_1+3\nu_3$	...	...	1665	1708
$3\nu_3+\nu_5$	...	...	1720	1753
$2\nu_5$	1811	1875	...	...
$\nu_1+\nu_2+2\nu_3$	...	...	1857	...
$\nu_1+\nu_5$	1859	1933	...	...
$2\nu_1$	1914	1991	...	...
$\nu_1+4\nu_3$	...	...	1919	1960
$4\nu_3+\nu_5$	...	...	1969	...
$\nu_3+2\nu_5$	2044	2116	...	...
$2\nu_1+\nu_6$	2084	2165	...	...
$2\nu_1+\nu_3$	2153	2228	...	...
$3\nu_1$	2853	2971	...	...

IV. DISCUSSION

A. Comparison to theory

The theoretical and experimental results are compared in Table I. It is apparent that the calculated band origins for the two electronic excited states are in excellent agreement with experiment, differing by a minimum of 5 cm^{-1} (0.02%) for the $\tilde{B}$ state of F_2BS and a maximum of 148 cm^{-1} (0.70%) for the $\tilde{B}$ state of Cl_2BS. We have previously[11] attributed a similar fortuitously good level of agreement in F_2BO to the small geometry changes on electronic excitation, the lack of spin contamination, and the predominantly single reference character of the wavefunctions, factors which also apply in the present cases. The measured vibrational fundamentals are very consistent with our CCSD(T)/aug-cc-pVnZ harmonic vibrational frequencies, with a maximum deviation of 35 cm^{-1} (3%) and an average error of only 7 cm^{-1}. The observed isotope shifts are also in excellent agreement with those calculated experimentally. Most importantly, the harmonic Franck-Condon simulations, which hinge on reliable molecular geometries, vibrational frequencies, and normal mode Cartesian displacement coordinates of the two combining electronic states, mimic experiment so well that they provide unambiguous identification of the emitting species and reliable assignments for the great majority of the emission bands.

B. Molecular structures

Since the spectra of F_2BO, F_2BS, and Cl_2BS are too congested for detailed rotational analysis, we must rely on the *ab initio* results to compare molecular geometries. The fact that the calculated rotational contours of the F_2BO and F_2BS $\tilde{B}$–$\tilde{X}$ 0_0^0 bands match experiment very well and that the Franck-Condon simulations agree so well with experiment in cases uncomplicated by extensive Coriolis or vibronic

TABLE VII. The *ab initio* ground state molecular structures of the known gas phase X_2BY free radicals and the calculated changes in geometry on electronic excitation.

Parameter		F_2BO [a]	F_2BS [a]	Cl_2BS [b]
	BY (Å)	1.3639	1.8019	1.7801
$\tilde{X}^2B_2$	BX (Å)	1.3135	1.3168	1.7544
	XBX (°)	119.29	120.56	120.89
	Δ[BY] (Å)	+0.042	+0.048	+0.068
$\tilde{A}^2B_1$	Δ[BX] (Å)	+0.002	+0.004	−0.007
	Δ[XBX] (°)	+1.44	−0.69	−2.23
	Δ[BY] (Å)	+0.011	+0.058	+0.064
$\tilde{B}^2A_1$	Δ[BX] (Å)	−0.006	−0.018	−0.021
	Δ[XBX] (°)	−0.09	+2.57	+4.93

[a]CCSD(T)/aug-cc-pV5Z values from Ref. 11.
[b]CCSD(T)/aug-cc-pVTZ values from this work.

coupling suggest that the *ab initio* structures are reasonably reliable. The structures obtained from theory are compared in Table VII. It is important to emphasize that each radical is predicted to be planar and of C_{2v} symmetry in all three electronic states.

It is immediately evident that the ground state bond angles in all three radicals are very similar and very close to the 120° value expected in the simplest approximation of sp^2 hybridization on the central boron atom. The BF bond lengths are almost identical in F_2BO and F_2BS, but the BS bond length of Cl_2BS is 0.02 Å shorter than that of F_2BS. The BF (1.31-1.32 Å) and BCl (1.754 Å) bond lengths are comparable to the bond lengths of BF_3 (1.307 Å) and BCl_3 (1.74 Å), respectively.[22,23]

Our LIF spectra reflect the changes in the molecular structure between the ground state and the $\tilde{B}^2A_1$ electronic excited state. Table VII shows that F_2BO undergoes very little geometry change and the LIF and absorption spectra consist of a prominent 0_0^0 band and little else. In F_2BS, the BS bond length elongates by about 0.06 Å and the bond angle opens by about 2.5°, resulting in additional absorption transitions to the 2^1 and 1^1 states, vibrations which both involve substantial BS stretching motions. In Cl_2BS, the changes are more global with a 0.06 Å elongation of the BS bond, a 0.02 Å decrease in the BCl bond length and an increase in the bond angle by 5°, which leads to activity in ν_1' (BS stretch), ν_2' (BCl stretch), and ν_3' (ClBCl bend).

The observed $\tilde{B}$-$\tilde{A}$ emission spectra reflect the geometric changes between the $\tilde{B}$ and $\tilde{A}$ states. These can be determined from the data in Table VII by taking the difference between the Δ values of the two states. For example, for F_2BS, we have $\Delta BS = \Delta[BY]\tilde{A} - \Delta[BY]\tilde{B} = 0.048 - 0.058 = 0.01$ Å. It is then immediately apparent that the only significant change is in the F_2B or Cl_2B bond angle, which accounts for the pronounced activity in the $\tilde{A}$ state ν_3 (symmetric bend or scissors) mode in all the spectra.

C. Vibronic coupling

Although the observed spectra of F_2BO and F_2BS show no evidence of vibronic coupling, the $\tilde{B}^2A_1$–$\tilde{X}^2B_2$ allowed electronic transition of Cl_2BS clearly contains forbidden components which gain intensity by vibronic coupling through the b_2 vibrations. Vibronic coupling can only occur between states that differ by no more than the species of one of the normal vibrations.[24] The involvement of the b_2 vibration implies that the $^2A_1$ state is coupled to a nearby $^2B_2$ state. Although it is, in principle, possible for the vibronic coupling to occur with the $\tilde{X}^2B_2$ ground state, it is so energetically distant (2.6 eV) that it is unlikely to be involved. Therefore, it must be that there is an excited $^2B_2$ electronic state of Cl_2BS sufficiently close to the $\tilde{B}$ state to cause the vibronic perturbations and that such a state does not substantially perturb the second excited state in the fluorinated compounds. Although no detailed calculations are available for the higher excited electronic states of Cl_2BS, MRCI calculations on the vertical spectrum of the isoelectronic H_2CO^+ species[25] predict a 2^2B_2 ($2b_2 \leftarrow 1b_2$) state about 1 eV above the $\tilde{B}^2A_1$ state, ideally situated for vibronic coupling. Similarly, in F_2CO^+, the 2^2B_2 state is within 0.3 eV of the 1^2A_1 state (calculated at the optimized ground state geometry of F_2CO) and within 0.8 eV according to the adiabatic ionization potentials from the photoelectron spectrum.[26] Of course, the 2^2B_2–$\tilde{X}^2B_2$ transition is also electronically allowed and so the forbidden component of the $\tilde{B}$-$\tilde{X}$ system of Cl_2BS can, at least in theory, gain intensity from the former by Herzberg-Teller intensity stealing. Detailed calculations of the identities and energies of the higher excited states of the X_2BY radicals will be required to further elaborate this point.

The $\tilde{A}^2B_1$ state cannot have a vibronic interaction with the nearby $\tilde{X}^2B_2$ state as C_{2v} molecules do not have a normal mode of a_2 symmetry.[24] In a similar fashion, although the evidence shows that the $\tilde{B}^2A_1$ state has an admixture of another $^2B_2$ state, this vibronic perturbation cannot lead to the occurrence of forbidden components in the $\tilde{B}^2A_1$–$\tilde{A}^2B_1$ emission band system and no such vibronically induced bands have been observed in the spectra of F_2BO, F_2BS, or Cl_2BS.

V. CONCLUSIONS

In the present case, high level *ab initio* theory has proven to be a powerful tool for predicting the spectroscopic signatures of new X_2BY free radicals, leading to their experimental detection in the gas phase. The Franck-Condon simulations of the emission spectra, in particular, were used to provide unambiguous identification of the radicals and, in most cases, reliable assignments of the observed transitions. The observed spectra of F_2BS are complicated by Coriolis coupling of the ν_2 and ν_4 modes in the excited state, so the 2_0^1 band emission spectrum exhibits transitions from both upper state levels. Even here, theory does very well—a composite Franck-Condon simulation of emission from 2^1 and 4^1 matches experiment very satisfactorily.

The LIF spectrum of Cl_2BS exhibits more vibronic activity than those of F_2BO and F_2BS, a necessary consequence of the larger geometric distortion of Cl_2BS on $\tilde{B}^2A_1$–$\tilde{X}^2B_2$ electronic excitation predicted by the *ab initio* calculations. In addition, Cl_2BS exhibits clear evidence of the existence of a forbidden component of the allowed electronic transition in

the experimental spectrum, involving activity in the b_2 modes, ν_5 and ν_6. This subset of the observed bands gains intensity by Herzberg-Teller intensity stealing from a nearby allowed transition, which is most likely 2^2B_2–$\tilde{X}^2B_2$. Finally, the Cl_2BS emission spectra are complicated by Coriolis coupling of ν_3 and ν_6 in the $\tilde{B}$ state. Both the excited state Coriolis coupling and vibronic interactions lead to complications in the $\tilde{B}$–$\tilde{X}$ emission spectra that cannot be accounted for in the harmonic Franck-Condon simulations. However, the $\tilde{B}$–$\tilde{A}$ band systems are largely free of such complexity and are reproduced by the simulations with gratifying fidelity.

ACKNOWLEDGMENTS

The research of the Clouthier group was supported by the National Science Foundation. P.M.S. would like to thank the Clouthier group for hosting his sabbatical leave.

[1]P. Renaud, A. Beauseigneur, A. Brecht-Forster, B. Becattini, V. Darmency, S. Kandhasamy, F. Montermini, C. Ollivier, P. Panchaud, D. Pozzi, E. M. Scanlan, A.-P. Schaffner, and V. Weber, Pure Appl. Chem. **79**, 223 (2007).
[2]S. H. Bauer, Chem. Rev. **96**, 1907 (1996).
[3]C. W. Mathews and K. K. Innes, J. Mol. Spectrosc. **15**, 199 (1965).
[4]C. W. Mathews, J. Mol. Spectrosc. **19**, 203 (1966).
[5]R. N. Dixon, G. Duxbury, R. C. Mitchell, and J. P. Simons, Proc. R. Soc. A **300**, 405 (1967).
[6]M. E. Jacox, J. Phys. Chem. Ref. Data **17**, 398 (1988).
[7]I. Baraille, C. Larrieu, A. Dargelos, and M. Chaillet, Chem. Phys. **282**, 9 (2002).
[8]R. Grimminger, P. M. Sheridan, and D. J. Clouthier, J. Chem. Phys. **140**, 164302 (2014).
[9]W. R. M. Graham and W. Weltner, Jr., J. Chem. Phys. **65**, 1516 (1976).
[10]E. L. Cochran, F. J. Adrian, and V. A. Bowers, J. Chem. Phys. **36**, 1938 (1962).
[11]D. J. Clouthier, J. Chem. Phys. **141**, 244309 (2014).
[12]W. W. Harper and D. J. Clouthier, J. Chem. Phys. **106**, 9461 (1997).
[13]D. L. Michalopoulos, M. E. Geusic, P. R. R. Langridge-Smith, and R. E. Smalley, J. Chem. Phys. **80**, 3556 (1984).
[14]E. L. Gamble, H. S. Booth, and H. Halbedel, *Inorganic Syntheses* (Wiley, 1950), Vol. 3.
[15]A. D. Becke, J. Chem. Phys. **98**, 5648 (1993).
[16]C. Lee, W. Yang, and R. G. Parr, Phys. Rev. B **37**, 785 (1988).
[17]T. H. Dunning, Jr., J. Chem. Phys. **90**, 1007 (1989).
[18]D. Feller, K. A. Peterson, and J. G. Hill, J. Chem. Phys. **135**, 044102 (2011).
[19]M. J. Frisch, G. W. Trucks, H. B. Schlegel *et al.*, GAUSSIAN 09, Revision A.02, Gaussian, Inc., Wallingford, CT, 2009.
[20]D.-S. Yang, M. Z. Zgierski, A. Bérces, P. A. Hackett, P.-N. Roy, A. Martinez, T. Carrington, Jr., D. R. Salahub, R. Fournier, T. Pang, and C. Chen, J. Chem. Phys. **105**, 10663 (1996).
[21]E. V. Doktorov, I. A. Malkin, and V. I. Man'ko, J. Mol. Spectrosc. **64**, 302 (1977).
[22]T. Masiello, A. Maki, and T. A. Blake, J. Mol. Spectrosc. **243**, 16 (2007).
[23]T. Wentink, Jr. and V. H. Tiensuu, J. Chem. Phys. **28**, 826 (1958).
[24]G. Herzberg, *Molecular Spectra and Molecular Structure III. Electronic Spectra and Electronic Structure of Polyatomic Molecules* (Van Nostrand, New York, 1966).
[25]P. J. Bruna, M. R. J. Hachey, and F. Grein, Mol. Phys. **94**, 917 (1998).
[26]F. Grein, J. Phys. Chem A **102**, 10869 (1998).